Pure Appl. Geophys. 181 (2024), 373–389

https://doi.org/10.1007/s00024-023-03394-9

Pure and Applied Geophysics

Understanding the Association of Tropical SST Anomalies on the ISMR During Extreme IOD Events

Shruti Verma,[1,2] R. Bhatla,[1,3] and Praveen Kumar Singh[3]

Abstract—The synergistic effects of the Indian Ocean Dipole (IOD) and El Nino Southern Oscillation (ENSO) have been investigated in this study over various subregions of India during 1981–2015. The IOD, is aperiodic and erratic, still this phenomenon is intrinsic in nature dependent on coupled ocean and atmospheric characteristics of the Indian ocean. About 60% of the IOD events showed its coexistence with ENSO during the 35-year recent climatology, still 40% of IOD events are independently occurring. For this analysis, the strongest three positive IOD (1994, 1997, 2006) and three negative IOD (1996, 1998, 2010) events have been identified that co-occurred with El-Nino and La-Nina events respectively. This study reveals that pIOD events are stronger and but the nIOD events are frequent and effecting Indian Summer Monsoon Rainfall (ISMR). The Sea Surface Temperature (SST) anomalies helps in explaining how strong pIOD favors moisture transport towards the western ghats, central India, northwest India, and anticyclonic conditions in the Bay of Bengal area whereas nIOD produces less rainfall in central India and the western ghats, but greater rainfall in the northeastern region. The reduced ENSO-IOD coupling in the 2000s may have strengthened the connection between ENSO and the Indian Summer Monsoon (ISMR), which had experienced a weakening in preceding decades, as reported by Kumar et al. (Science 284:2156–2159, 1999) and Ashok et al. (Geophys Res Lett 28:4499–4502, 2001). This study also investigates whether a regional climate model (RegCM4.7) accurately incorporate the realistic ENSO-IOD coupling mechanisms, and simulate its impact on regionalized precipitation during summer monsoon. The high-resolution RegCM4.7 simulations are close to the observation of rainfall during 2006, 1996 and 2010 extreme IOD events simulation that indicate RCM's higher sensitivity towards the abrupt change in boundary condition such as SST. Overall, the monsoon core regions i.e., central India, western ghats and northeast India, both IOD and southern oscillations are the synergistic predictor for the ISMR.

Keywords: Indian ocean dipole (IOD), sea surface temperature (SST), Indian ocean (IO), regional climate model (RegCM), Indian summer monsoon rainfall (ISMR).

1. Introduction

Since the 1950s the tropical Indian Ocean (IO) Sea surface temperature (SST) marked as a gradually increasing trend (Du & Xie, 2008; Solomon et al., 2007) and will continue rising in SST with increasing Greenhouse gas emissions (Vecchi & Sodan, 2007). The rising SST produces a phenomenal dipole behavior in the tropical IO i.e., termed the 'Indian Ocean Dipole (IOD)'. The IOD also known as the Indian Nino, is a periodic oscillation of SSTs in which the western IO becomes warmer (positive phase) and then colder (negative phase) than the eastern part of the ocean. The IOD is characterized by an aperiodic oscillation of sea-surface temperatures (SSTs) between "positive," "neutral," and "negative" phases. A positive phase is characterized by higher-than-average SST and precipitation in the western IO region, as well as a cooling of waters in the eastern Indian Ocean, which causes droughts in neighboring land areas of Indonesia and Australia. The negative IOD's (nIOD) phase causes the opposite circumstances, with warmer water and more precipitation in the eastern Indian Ocean and colder, drier temperatures in the west.

The IOD is one of the tropical Indian Ocean's major modes of variability, which was identified and named by climate researchers at the end of the 1990s (Saji et al., 1999; Webster et al., 1999). The IOD has been identified as an El-Nino Southern Oscillations (ENSO)-forced mode of oscillation (Chattopadhyay

[1] Department of Geophysics, Institute of Science, Banaras Hindu University, Varanasi, India. E-mail: shrutivermama072@gmail.com; rbhatla@bhu.ac.in

[2] Department of Atmospheric Physics, Faculty of Mathematics and Physics, Charles University, Prague, Czech Republic.

[3] DST-Mahamana Centre of Excellence in Climate Change Research, Institute of Environment and Sustainable Development, Banaras Hindu University, Varanasi, India. E-mail: praveenkumarsingh1564@gmail.com

& Bhatla., 1996; Allan et al., 2001; Baquero-Bernal et al., 2002; Dommenget, 2011; Huang & Kinter, 2002; Zhao et al., 2019), as well as a self-sustaining mode of oscillation (Ashok et al., 2003; Behera et al., 2006; Behera et al., 2006; Fischer et al., 2005; Wang et al., 2019; Yamagata et al., 2004). Changes in the frequency and teleconnections of the IOD in the past have been observed on long-term recordings (e.g., Abram et al., 2020). Early phases of the Indian Ocean Dipole (IOD), despite generally having weaker intensities compared to normal and prolonged IOD events, still have a substantial impact on boosting the Indian Summer Monsoon (ISMR). The Indian monsoon consider as lifeline for the region, impacting agriculture, economy, water resources, and the overall well-being of the population.

This effect is attributed to increased evaporation in the Arabian Sea and the presence of a stronger cross-equatorial flow during these early positive IOD years (Anil et al., 2016). However, the precise mechanism underlying the coupling between ENSO and IOD remains unclear, contributing to the varying findings in previous literature regarding their interaction. Allan et al. (2001) proposed that while there is a degree of IOD variability linked to ENSO, certain IOD events could be triggered by processes within the Indian Ocean (IO) that are not reliant on ENSO. Lau and Nath (2004) suggested that certain IOD occurrences might arise from inherent air-sea interactions within the Indian Ocean, while others could be triggered by the ENSO.

Studies have revealed that in recent decades, the coupled air-sea interaction caused by a strong positive IOD (pIOD) (Saji et al., 1999; Webster et al., 1999) has also affected Indian Summer Monsoon Rainfall (ISMR) variability (Ashok & Saji, 2007; Ashok et al., 2001). During the majority of the pIOD years, ENSO-induced anomalous subsidence is decreased by IOD-induced convergence, compensating for ENSO's weakening influence on monsoon (Ashok et al., 2001; Guan & Yamagata, 2003; Guan et al., 2003). The IOD, on the other hand, evolves during the boreal summer monsoon season and has a connection with rainfall during the monsoon season, therefore it has no predictive value before the monsoon season. The relationship between pIOD and above normal rainfall does not exist for all pIOD years (Ashok et al., 2001), this suggests that both large-scale ENSO forcing and local air-sea interaction over the tropical IO are equally significant for ISMR variability.

A weakening of the ISM-ENSO connection was discovered at the close of the twentieth century (Kinter et al., 2002; Kumar et al., 1999) with the IOD recognized as a possible cause of ISMR. Several articles investigated the individual and combined impacts of ENSO and IOD on ISMR and discovered that both phenomena, both separately and in combination, have an impact on ISMR performance (Ashok et al., 2004; Bhatla et al., 2020, 2023; Hrudya et al., 2020; Krishnaswamy et al., 2015; Li et al., 2017; Sikka & Ratna, 2011).

The thermocline warming was caused by anomalous ocean downwelling in the southwest tropical IO induced air convection, resulting in an easterly wind anomaly along the equator, and the positive feedback resulted in an IOD event (Du et al., 2020). Furthermore, the record-breaking interhemispheric pressure gradient across the Indo-Pacific area produced northward cross-equatorial flow over the western Maritime Continent, which was capable of triggering significant wind-evaporation-SST and thermocline feedbacks that contributed to the high IOD (Lu & Ren, 2020). It is expected that the western IO will warm at accelerated rates due to climate change (Zheng et al., 2013) leading to an increasing occurrence and intensity of pIODs (Cai et al., 2018).

The optimistic view of this study is (i) to examine the association of IOD events with ENSO over India (ii) to describe the characteristics and duration and intensity of the extreme IOD events based on the time evaluation and its structure (iii) the understand the distinct role of major IOD event in modulating the ISMR over India and its different sub-regions.

2. *Data and Methodology*

The intensity of the IOD is represented by anomalous SST gradient between the western equatorial IO (50° E–70° E and 10° S–10° N) and the south eastern equatorial IO (90° E–110° E and 10° S–0°) it usually developing in summer, maturing in autumn, and decaying in winter (Saji et al., 1999)

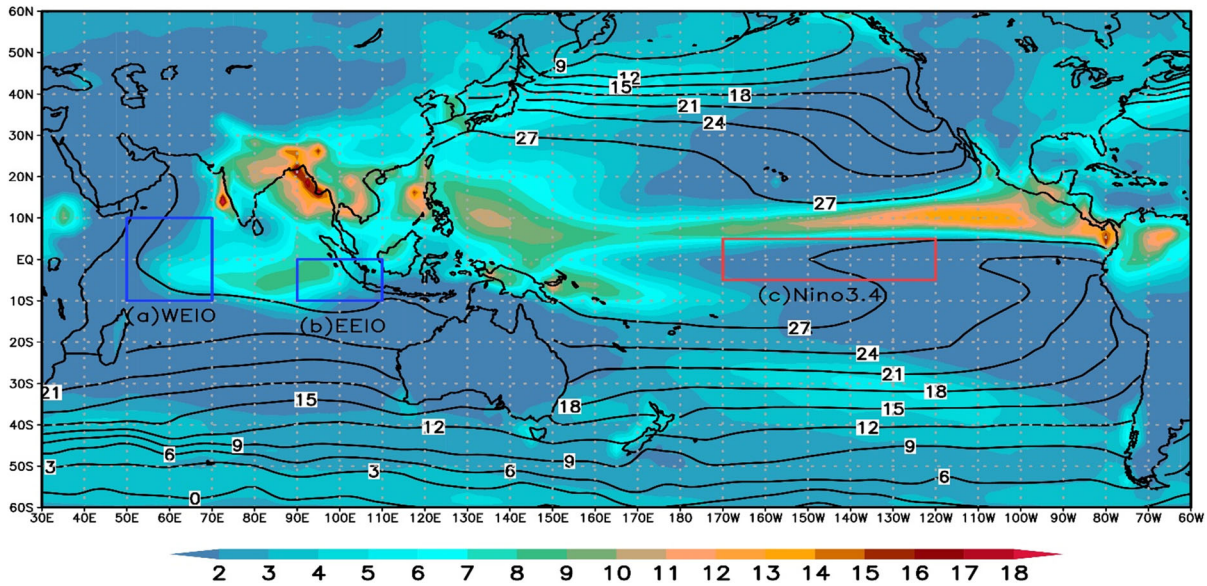

Figure 1
Global sea surface temperature (°C; contour) and precipitation (mm/day; shaded) during June, July, August and September (1981–2015) where three sub domains indicate **a** west equatorial Indian ocean (WEIO); **b** east equatorial Indian Ocean (EEIO) and **c** Nino3.4 region regions

(Fig. 1). This gradient is named as Dipole Mode Index (DMI), which predict the occurrence of an IOD based on ± 1 standard departure of September–October–November (SON) average DMI. When the DMI is positive then, the phenomenon is refereed as the pIOD and when it is negative, it is refereed as nIOD. DMI have been calculated using Extended Reconstructed SST, version 3b (ERSST.v3b) based on 1981–2015 climatology. Based on the intensity and duration of DMI value major/extreme pIOD (1994, 1997, 2006) and nIOD (1996, 1998, 2010) are selected from Fig. 2 and Table 1. Additionally, we incorporated sea surface salinity (SSS) ocean reanalysis dataset, known as The Ocean ReAnalysis System 5 (ORAS5) provided by the European Centre for Medium-Range Weather Forecasts (ECMWF) (Zuo et al., 2019). The rainfall subregion/zones described in Table 2 viz *North west India (NWI), Northcentral India (NCI), Western peninsular India (WPI), Eastern peninsular India (EPI) and Southern peninsular India (SPI)* (Bhatla et al., 2019; Verma et al., 2021).

The ENSO life cycle for the corresponding to the pIOD and nIOD tabulated in Table 3 which helps in explaining the association of ENSO and IOD response. The El Nino years were identified based on the June to September average SST anomaly over the Nino3.4 region. The identification of ENSO years and climatology distribution of rainfall based on Nino3.4 SST anomaly Index (170° W–120° W 5° S–5° N,) during Northern Hemispheric summer (June–September: JJAS) 1981–2015. As per the definition, El Nino refers to a situation where five consecutive three months moving average Oceanic Nino Index Average (ONIA) values above 0.5 °C, whereas for the La Nina condition the ONIA value is below − 0.5 °C (Table 2).

The *state-of-the-art* in the regional climate model RegCM has contributed significantly to the scientific society towards the study of climate change and its variability (Giorgi et al., 2012). The Abdus Salam International Centre for Theoretical Physics regional climate model RegCM4.7 (version 4.7) (Giorgi et al., 2012) have been used which is driven by ERA-Interim reanalysis data at a grid spacing of 25 km over the SA-CORDEX domain (Table 3). The latest hydrostatic version of RegCM4.7 has been considered with mixed cumulus parameterization

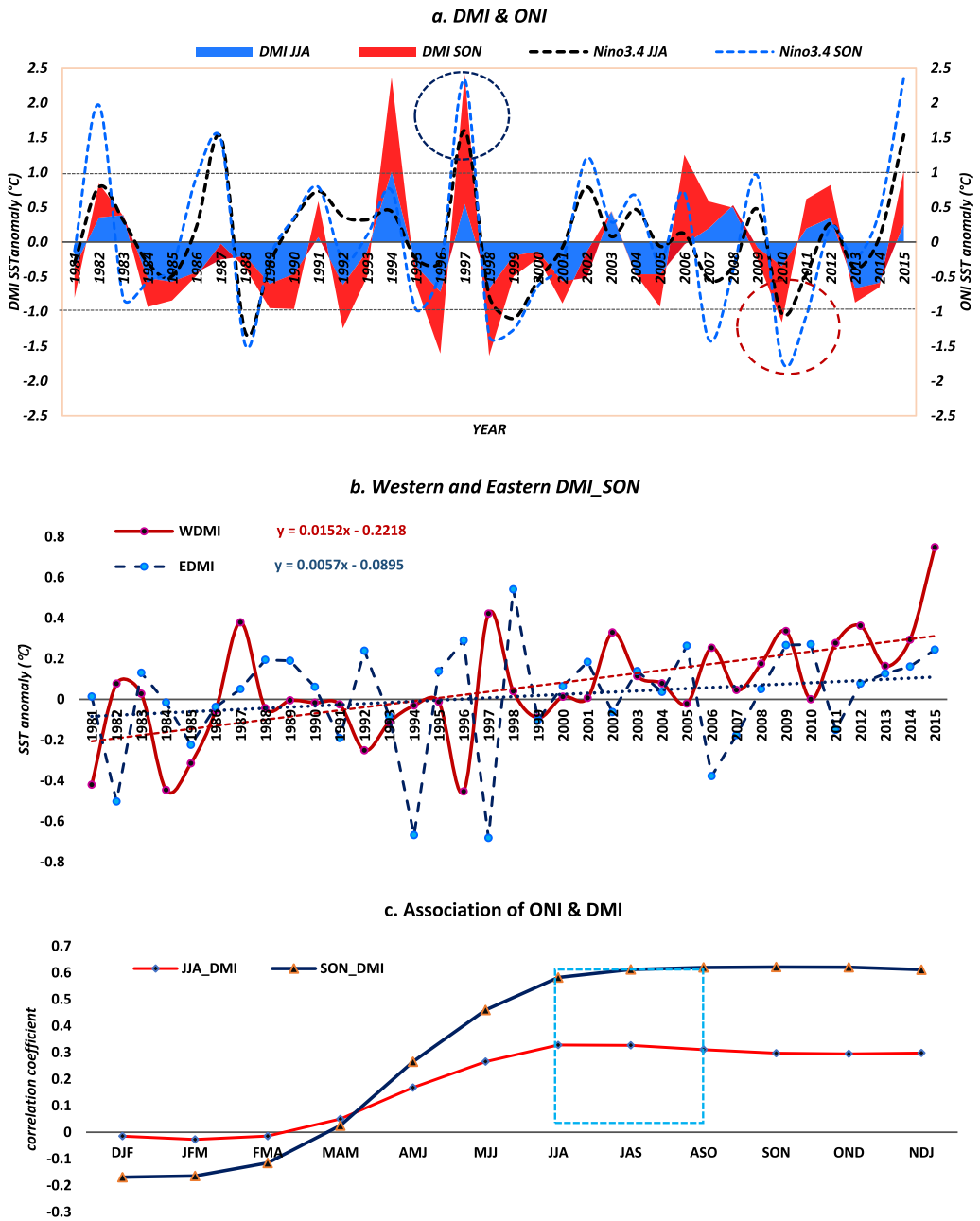

Figure 2

a–c Year to year SST variation of **a** Dipole mode index (DMI) and Oceanic Nino Index (ONI) for JJA and SON; **b** variability and trend of Western & Eastern DMI (SON); **c** correlation coefficients between IOD index (DMI for JJA & SON) and Oceanic Nino index (ONI) during 1981–2015

scheme i.e., Emanuel over Land & Tiedtke over Ocean. Model implemented the Holtslag scheme (Holtslag et al., 1990) as planetary boundary layer schemes. The radiation scheme is NCAR's community climate model version 3, land surface parameterization given by Biosphere–Atmosphere Scheme and Zeng's ocean flux scheme for ocean flux parameterization. The subgrid explicit moisture

Table 1

List of positive and negative Indian Ocean dipole (IOD) years along with ENSO event during 1981–2015

Positive IOD		Negative IOD	
Strong	Moderate/Weak	**Strong**	Moderate/Weak
1994 (MEN)	**1982 (SEN)**	1996 (WLN)	1984 (WLN)
1997 **(SEN)**	2012 (N)	**1998 (SLN)**	1989 (N)
2006 (WEN)	**2015 (SEN)**	**2010 (SLN)**	1992 (N)
			2001 (N)
			2005 (WL)
			2013 (N)

Positive IOD and Negative IOD, Based on ± 0.5 deviation of Dipole Mode Index (DMI) during September–October-November

WEN Weak El Nino, *MEN* Moderate El Nino, *SEN* Strong El Nino, *WLN* Weak La Nina, *MEN* Moderate La Nina, *SEN* Strong La Nina, strongest event highlighted in 'bold'

Table 2

ENSO life cycle and standardized rainfall departure for strong pIOD and nIOD during JJAS

	Year	ENSO life cycle*	AIR	CIR
pIOD	1994	Developing	**1.32**	**2.9**
	1997	mature	0.0	0.19
	2006	Developing	0.60	0.40
nIOD	1996	Decaying	0.02	0.34
	1998	mature	0.42	− **0.44**
	2010	mature	0.66	− **0.92**

Bold values indicate the Stronger standardized rainfall departure

*ENSO life cycle; developing, mature and decaying phase

AIR All India rainfall; *CIR*, Central India rainfall

scheme is used for the large-scale precipitation scheme (Pal et al., 2000). With this model configuration, six set of simulation have been carried out specifically for extreme pIOD (1994, 1997 & 2006) and nIOD (1996, 1998 & 2010) over SA-CORDEX domain.

3. Results and Discussion

This study presents a detailed description of interannual variation of DMI and ONI during 1981–2015 during JJA and SON. Figure 2a–c represent intensity, trend and association of ONI with DMI during south west monsoon period, based on this extreme pIOD (1994, 1997 & 2006); nIOD (1996, 1998 & 2010) have been selected for the study. After that, seasonal SST and surface pressure anomaly has been described during the extreme pIOD and nIOD years.

Table 3

RegCM4.7 model configuration

Dynamics	Hydrostatics (MM5)
Domain	South Asia CORDEX domain (22° S–50° N; 10° E–130° E)
Horizontal resolution	25 km horizontal
Vertical level	23 sigma level
Planetary boundary layer scheme	Holtslag PBL
Initial and boundary conditions	ECMWF ERA Interim reanalysis
Cumulus parameterization scheme	Emanuel over Land + Tiedtke over Ocean
Radiation scheme	NCAR's CCM3
Ocean flux parameterization	Zeng's ocean flux
Large-scale precipitation scheme	SUBEX
Land surface parameterization	BATS

3.1. The Interannual Variability of Seasonal Dipole Mode Index (DMI) and Oceanic Nino Index (ONI)

The temporal variability of DMI and ONI indices that monitor ENSO and IOD events, respectively have been illustrated in Fig. 2a for the period of 1981–2015 (JJA-SON). The year-to-year variability and trend analysis are necessary to monitor the fluctuation of SST during IOD and ENSO. This temporal interannual variability of DMI represented the pIOD (above 0.5 °C; 1982, 1994, 1997, 2006, 2012 & 2015) and nIOD (below − 0.5 °C; 1981, 1984, 1989, 1992, 1996, 1998, 2001, 2005, 2010 & 2013,) in which bold one is extreme IOD cases. The year 1994 exhibited the strongest DMI during 1981–2015, but the ENSO (Moderate El Nino) was in the developing stage, thus the AI rainfall was above normal (1.32 SD departure) and CI (Central

India) received anomalous heavy rainfall (2.9 SD departure)/flood like condition. The study can verify that strong pIOD can sustain and affect the ISMR, without associated with El Nino (Ashok et al., 2003).

The case of 1997, when a strong El Nino (2.3 °C ONI) occurred concurrently with strong pIOD (2.3 °C) (Ashok et al., 2001; Gua et al., 2015), this is the single case study of pIOD when both pIOD and mature stage ENSO coincide with each other with same intensity Table 2. So strong El Nino effect of the ISMR nullify by the strong pIOD helps in developing a normal monsoon year. Hence, it is crucial to consider the ENSO phase when analyzing the impact of IOD on the ISMR. In the year 2006 ENSO lifecycle was in the developing phase and its was in the weak phase, but the DMI SST anomaly peaked during SON (1.3 °C) therefore a normal monsoon occurs with good rainfall over CI. Overall, IOD is aperiodic in nature, not a definite pattern related to the occurrence of strong pIOD and ENSO, but the coherence of the ENSO-IOD life cycle helps in modulating ISMR, With the help of this analysis, it can be concluded that when weak/moderate ENSO event coincides with the strong DMI during JJA/SON affect the ISMR.

Similarly, the strong nIOD events are selected to understand the coherence of ENSO with IOD, although nIOD events are more frequent but in terms of strength its lower than pIOD. Strong nIOD such as 1996, 1998 and 2010 has been analyzed with respective year ENSO events. The year 1998 and 2010 (nIOD) are extreme in nature coinciding with the very strong La-Nina event thereafter produced a negative impact on the CI during ISMR. The AIR during 1998 and 2010 were in the normal category, but other regions such as CI were affected by the severity of the nIOD event. Another possible explanation of the effect of the nIOD (1998 and 2010) states that the mature stage of the La Nina event starts from JJA-SON.

Figure 2b elucidates the interannual variability and trend of Western DMI and Eastern DMI of SON. The warming of tropical IO SST is mentioned in several studies, after the 1950s, the tropical IO SST warming trend is a major robust warming region in the past six decades (Du & Xie, 2008). Similarly, the WDMI SST trend has been more frequently increasing with the slope of 0.015 °C/year), however, the increasing trend of EDMI SST is 0.005 °C/year not significant as WDMI during 1981–2015. Trenberth, 1990 highlights the regime shifting in global climate patterns due to global warming. It also includes the abrupt decadal variability of coupled atmosphere–ocean system which may enhance the IOD variability (Zheng et al., 2010). In Fig. 2a and b, the year-to-year fluctuations in WDMI, EDMI, and Nino3.4 provide an explanation for the diminishing connection between ENSO and IOD. This reduction in their association is attributed to the initiation of positive IOD events driven by the negative sea surface temperature anomalies in the eastern IO, a phenomenon supported by prior research (Li et al., 2003; Sooraj et al., 2009; Ham et al., 2017). The stronger warming in the central Pacific during the Central Pacific El Niño, a phenomenon that became more frequent in the 2000s, has the potential to diminish the usual influence of the positive ENSO-IOD relationship. Thus, the substantial reduction in the connection between ENSO and IOD during the 2000s and 2010s can be attributed to variations in how ENSO develops (Table 2). This diminished association between ENSO and IOD may have contributed to a decrease in the IOD's intensity during the months of September to November (SON) in recent decades Fig. 2a, b.

In Fig. 2c explained the variation of correlation coefficient value between the ONI (DJF-NDJ) with DMI of JJA and SON during the considered period. Although it has been clear that IOD is aperiodic oscillation, there is a seasonal pattern of association between its indices ONI and DMI, which have been displayed with the help of a correlation coefficient. Initially, when the formation of ONI took place over the pacific Nino3.4 region, it was showing a negative correlation with both seasons DMI i.e., − 0.2. But the positive association between both indices start appearing after MAM (greater than 0) after that, JJA to NDJ it was showing a positive association (correlation coefficient greater than 0.5).

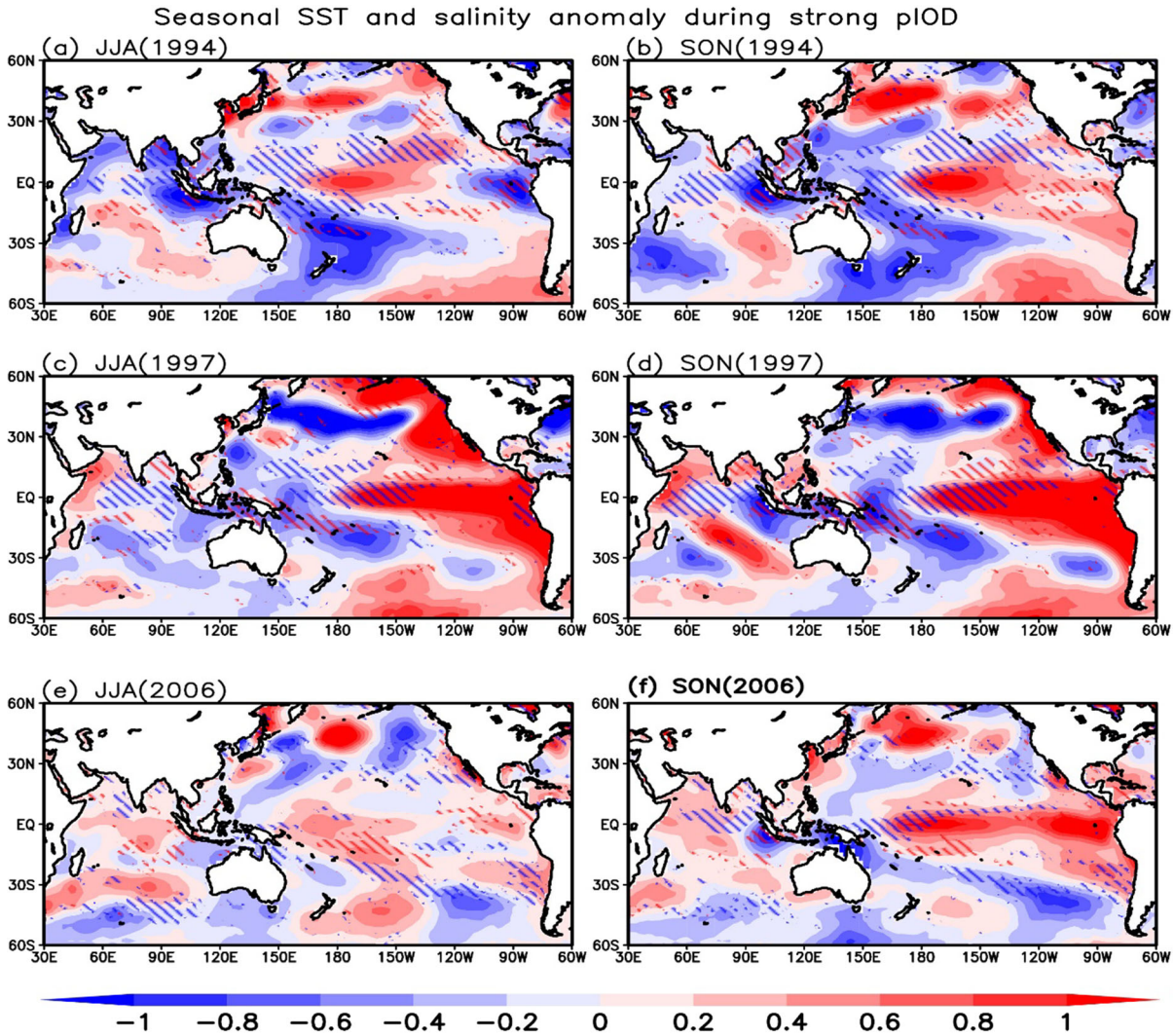

Figure 3
a–f Seasonal (JJA & SON) sea surface temperature (°C; shaded) and sea surface salinity (psu; blue(− ve) and red (+ ve) strips) anomalies for extreme pIOD years **a**, **b** 1994; **c**, **d** 1997 and **e**, **f** 2006

3.2. The Response of Seasonal Mean Anomalies in SST and SSS During Major pIOD and nIOD

The Indian and Pacific Ocean SST patterns (shown in Fig. 3) indicate the Indo-Pacific warm pool during the JJA (June, July, and August) and SON (September, October, and November) seasons, which are associated with the majority of severe precipitation occurrences across the South Asian region (Pillai & Annamalai, 2012). The composite plot displays three distinct extreme pIOD years (1994, 1997 and 2006) associated with El Nino events. Strong pIOD and El-Nino both contribute to cooling in the region between Sumatra and Papua New Guinea, driving the ITCZ in the eastern Indian Ocean to shift southward (Reed et al., 2019). The extensive cooling of this region due to El-Nino favors anti-cyclonic conditions in the Bay region, while warmer SST towards the western equatorial IO leads to strong easterlies over the equatorial IO, pushing the cross-equatorial monsoon winds, whereas the warmer temperature along the Arabian Sea region

favors more moisture transport towards the subcontinent (Ueda, 2005).

The 1994 temperature pattern indicates an El-Nino event with below-normal surface temperature across the Malacca Strait during JJA, inducing subsidence in the eastern Indian ocean region and finally leading to an easterly flow around the equator that blends with the Arabian sea branch of the monsoon (Ashok et al., 2004; Sikka & Ratna, 2011). Moreover, the lower temperatures in the BoB region result in less moisture advection for winds travelling north-east India and Bangladesh. The high temperature in the eastern Pacific during JJA 1997 resembles a strong El Nino event, which usually results in westerly winds over the Pacific and weaker easterlies along the equatorial IO, but the higher temperature along the western IO and Arabian sea ensures wind divergence from the Eastern Indian Ocean towards the Arabian sea. However, higher temperatures in the BoB in 1997 made conditions more suitable for stronger winds and enhanced moisture advection towards the Indian subcontinent.

El-Nino conditions prevailed in the Pacific throughout the JJA months of 2006, although the temperature gradient was less prominent, whereas the pIOD caused higher SST along the Indian Ocean's equatorial and northern parts. Because of the temperature difference, winds from northern Australia travel westward, crossing the warm Indian Ocean to combining with the summer monsoon branches of the Arabian Sea and the BoB. As a result, the ISM's performance is associated to its evolution between June and July, with westward passage of cloud bands from the eastern Indian ocean and west Pacific, boosting normal to good monsoon prospects due to favorable temperature in the western IO during pIOD years (Krishnan et al., 2011; Krishnaswamy et al., 2015). During the initial stage of pIOD in the months of June to August, positive SSS anomalies are found along the off the coast of Java and Sumatra coast that are due to the combination of wind-driven upwelling of subsurface high-salinity waters, enhanced evaporation, and anomalous surface circulation (Fig. 3a, c and e). The reduced precipitation in the region as notable feature during the pIOD which account positive SSS anomaly. In the advance and mature phase of pIOD, occurring during September–November (Fig. 3b, d and f) we observed that reinforcement of negative salinity anomalies with the intensified southwestward currents and these negative salinity anomalies expand all the way to the southwestern IO (Yuhong et al., 2013). Simultaneously, positive SSS anomalies reach their highest strengths off the coasts of Java and Sumatra.

Figure 4 illustrates three nIOD years (1996, 1998 and 2010) that corresponded with La Nina episodes. The westward drag of the trade winds throughout the equatorial IO is resisted by considerably lower SST over the western IO, and the surface fluxes give rise to moist stability and so below-normal rainfall in the region (Annamalai, 2010). In 1996, the temperature gradient over the equatorial IO was rather large (Fig. 3a, b), resulting in a reduced push for the monsoon winds, which move southeasterly from the Mascarene high and southwesterly after reaching the equator. The Arabian Sea was anti-cyclonic during the JJA of 1996 (Fig. 3a), which is detrimental for the monsoon winds, especially the Arabian Sea branch of the ISM, since the lower temperature hinders moisture acquisition by the winds as they travel towards the western ghats, west-central and CI (Thompson et al., 2009) (Fig. 4d).

Later in 1996, conditions in the western IO, including the Arabian Sea, were more anti-cyclonic and extended into the BoB area (Fig. 3b), resulting in lower-than-average rainfall throughout the majority of the subcontinent (Fig. 4d). These circumstances yield abnormal anti-cyclonic circulations in response to Rossby wave in the near surface atmosphere, and advection of winds with lower moisture content from the subtropics towards the subcontinent takes place (Annamalai, 2010). The 1998 La Nina was substantially stronger and the nIOD added up to the average temperature and salinity around Sumatra Island in the equatorial IO (Fig. 3c–d). The nIOD of 1998 was not as robust, but it was sufficient enough to resist winds away from India's western coast and limit moisture transfer during JJA (Fig. 3c), while conditions deteriorated later in SON (Fig. 3d). During the JJA of 1998, however, there was increased convergence and surplus precipitation across the south-east Asian area, including north-east India, due to higher SST. The co-occurrence of nIOD and a strong La Nina, the whole IO was warm in 2010, with the eastern IO being even

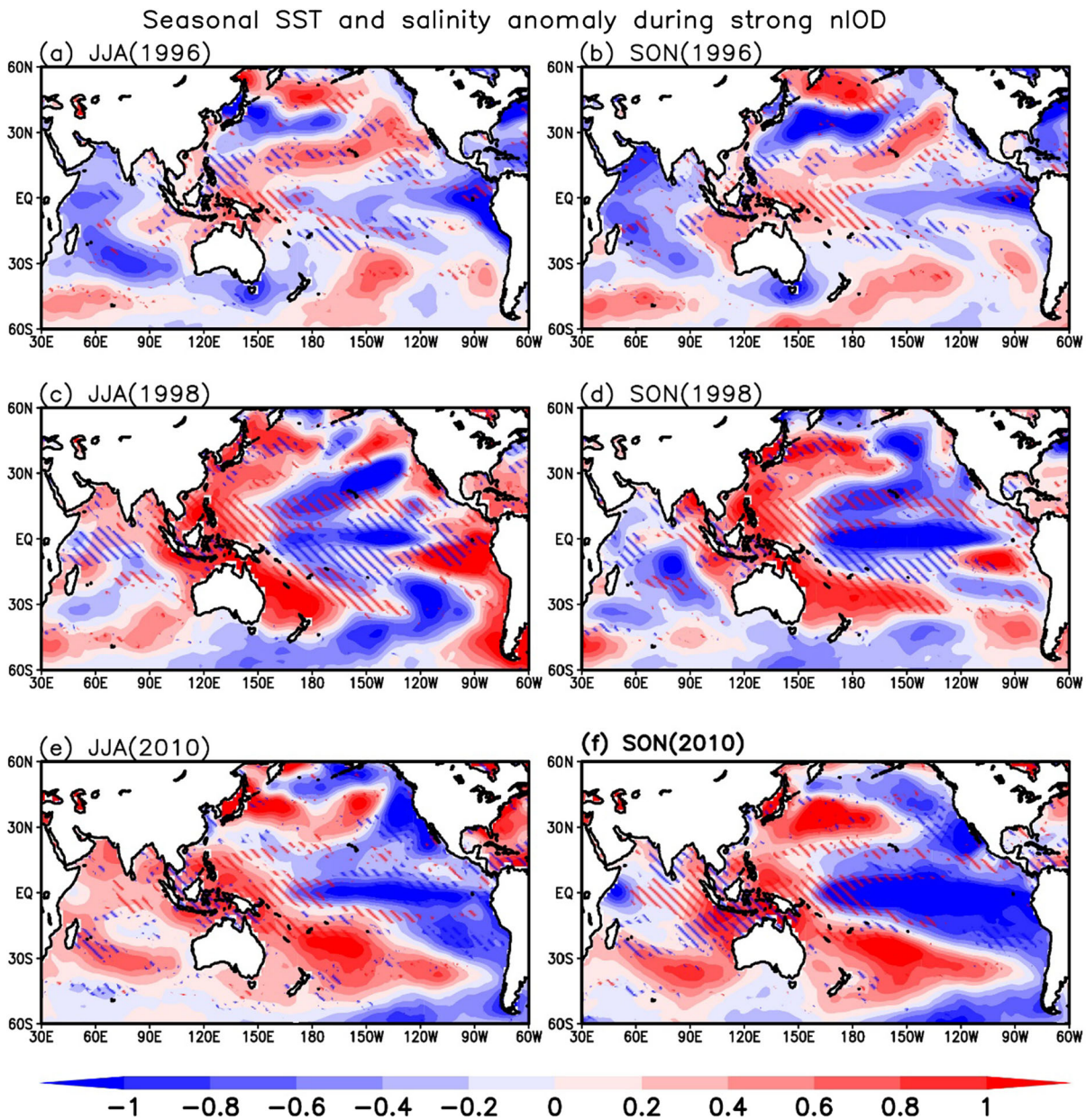

Figure 4
a–f Seasonal (JJA & SON) sea surface temperature (°C; shaded) and sea surface salinity (psu; blue(− ve) and red (+ ve) strips) anomalies for extreme nIOD years **a**, **b** 1996; **c**, **d** 1998; **e**, **f** 2010

warmer than the western ocean (Fig. 3e, f). Conditions in 2010 were similar to 1998, but the southern warming of IO created a weak Mascarene high, resulting in a substantially negative rainfall anomaly in central and eastern India (Fig. 6f) due to a reduced temperature gradient towards the subcontinent, responsible for northward propagation of summer monsoon (Fig. 4f). During JJA positive anomalies in SSS became evident in the central EIO, with their peak occurring in SON (Fig. 4e–f). The increase in SSS can be attributed to anomalous currents that transported high-salinity water eastward along the

equator. Simultaneously, due to suppressed upwelling off the coasts of Java and Sumatra caused negative SSS anomalies and increased precipitation during 2010 (Du and Zhang 2020).

3.3. Possible Dynamics of the Two Distinct Extreme pIOD and nIOD Regimes in Observations

The slowly varying boundary condition such as SST and sea surface salinity (SSS) anomaly and ENSO driver are common phenomena helps in understanding the dynamics involves in the formation of two distinct type extreme pIOD and nIOD.

3.3.1 Role of SST-Wind Anomaly

The establishment of IOD events begins with SST anomalies that respond to surface wind anomalies (Behera et al., 2006; Saji & Yamagata, 2003). Surface heat fluxes also have a significant role in the development and termination of IOD (Thompson et al., 2009). 'Bjerknes feedback' occurs due to the coupling interaction between the SST and wind which plays a critical role in the IOD development process. During a pIOD event occurs, a cold-water anomaly and southeasterly wind anomalies are encountered along Jawa–Sumatra and in the south-eastern TIO, respectively. These wind anomalies induce upwelling and tilt the thermocline, both effect cools the equatorial IO and suppress atmospheric convection eventually raises the sea level pressure and intensifying the easterly winds at the surface. In the subsequent months, the eastern cold-water anomaly extends toward the equator along the Indonesian coast and affects the Walker circulation through the Bjerknes feedback. Thus, easterly wind anomalies gradually emerge in the central TIO, and the western tropical IO gradually warms.

3.3.2 ENSO Driver

The combined response of ENSO and IOD adds another intriguing dimension to comprehending this intricate phenomenon. It has been renowned that ENSO far-flung forcing leads to an Indian Ocean basin scale warming in the following spring after the ENSO matures (Xie et al., 2002). Nearly 40% of IODs occur simultaneously with ENSO; the pIOD is associated with El Niño and the nIOD generally with La Niña (Ashok et al., 2004; Saji & Yamagata, 2003) but it can happen independently also. It was also recently verified that the ENSO-IO coupling is different for warm and cold events. With the help of numerical simulations, it shows that the large-scale atmospheric circulation which initiates IOD is different for the ENSO associated and non-ENSO associated IODs (Lau & Nath, 2004). Thus, the evolution of spatial structure of IOD for positive and negative phases as well as with and without ENSO helps in unfolding the complexity within these coupled phenomena.

The possible mechanism involves for the influence of IOD on the ENSO have been presented in various studies which occur with the help of atmospheric bridge and oceanic pathways (Annamalai et al., 2005; Wieners et al., 2016). In the atmosphere modulation in the low-level zonal wind over the equatorial pacific observed through walker circulation or due to Philippine Sea anticyclone. That means, the warm SST anomaly in the western IO enhance the local convection, and eventually suppress the convection over the Indonesia and helps in weakening the walker circulation over tropical Pacific. Which on the other hand, alarms Philippines Sea anticyclone and generate kelvin wave this it modulates the western pacific circulation. Thus, these two processes cause modulation in the surface zonal wind in the tropical pacific and eventually can affect the development of ENSO. Thus, both climatic events can overrule each other through tropospheric biennial oscillation (Meehl et al., 2003).

3.3.3 Role of Salinity

Sea surface salinity (SSS) variation is an important factor of the IOD that contributes significantly to its formation through positive feedbacks that enhance temperature variations and drive IOD circulation across the TIO. The IO experiences relatively milder and shorter-lasting SSS anomalies, lasting less than two months, during El Niño events compared to dipole events, as described by Vinayachandran and Nanjundiah (2009). The limited impact of ENSO on SSS emphasizes the utility of SSS as a valuable

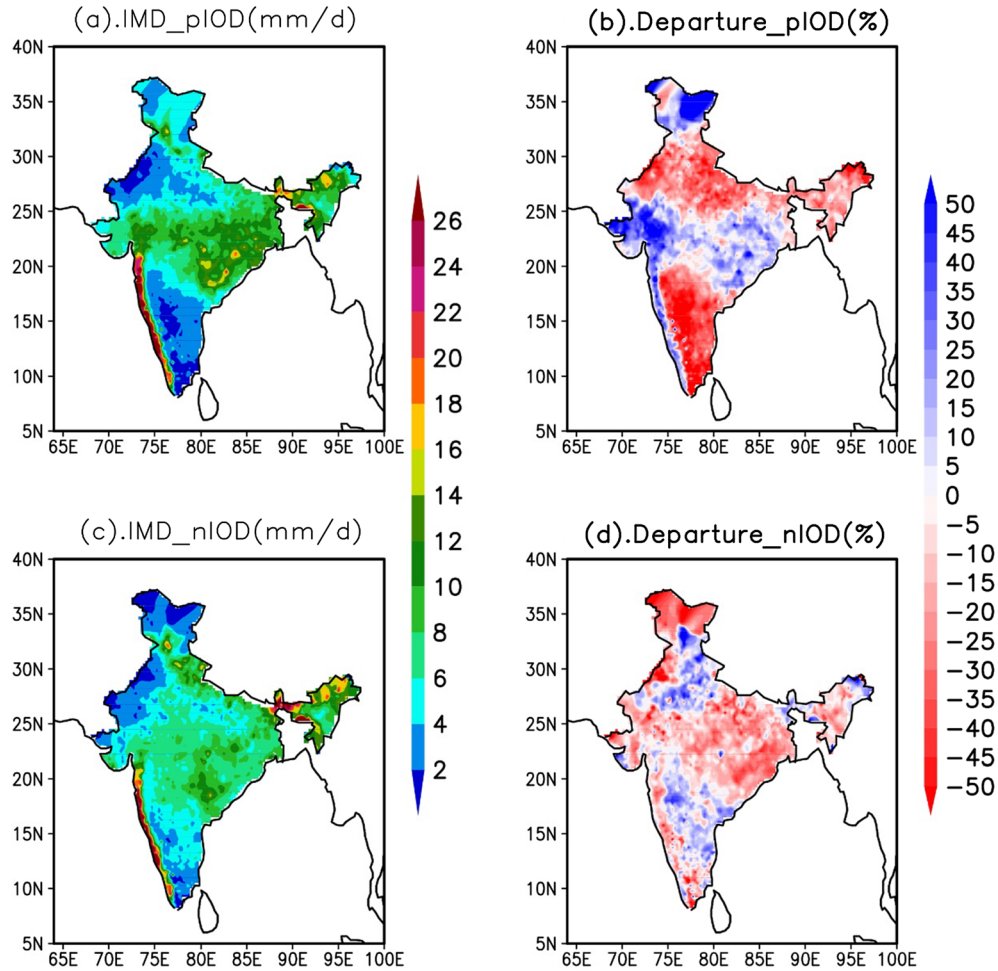

Figure 5
a–d Observed (IMD) seasonal mean (JJAS) rainfall and its departure (in %) from the normal rainfall for extreme pIOD and nIOD events during 1981–2015

variable for enhancing our understanding of IOD. Previous Study of Webster et al., 1999 illustrated that the effect of salinity on SST anomalies is to create areas of enhanced or reduced convection, resulting in precipitation anomalies across equatorial IO and vice versa precipitation anomalies also act to increase or decrease SSS anomalies. During pIOD significant reduction in SSS in the central eastern EIO, while the southeastern IO (Sumatra coast) exhibits atypical high SSS reported in this paper also confirmed by the previous studies of (Kido et al., 2019; Yuhong et al., 2013). The SSS pattern during nIOD evets are completely different their positive counter parts and depicting slow progression and transportation of SSS eastward across the equator (EIO). Nonetheless, research indicates that this pattern can also be observed during neutral IOD years. Consequently, it presents challenges in terms of comprehension and monitoring when relying solely on SSS anomalies.

3.4. Spatial Distribution of Summer Monsoon Rainfall and its Departure During Extreme pIOD and nIOD

The mean and departure in rainfall during three pIOD and nIOD have been analysed using the gridded IMD rainfall data in Figs. 5a–d and 6a–f. The ISMR distribution during the extreme pIOD

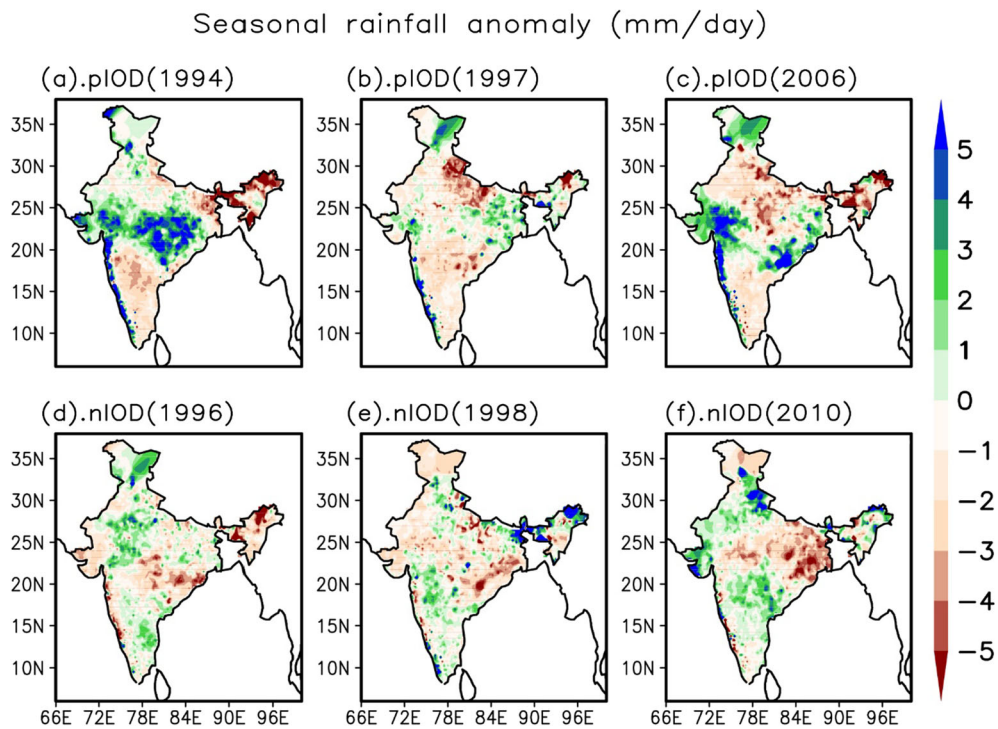

Figure 6
a–f Observed (IMD) seasonal mean (JJAS) rainfall departure (unit in mm/day) from the normal monsoon rainfall for pIOD **a** 1994; **b** 1997; **c** 2006 and nIOD **d** 1996; **e** 1998; **f** 2010

years explains that WG, CI and NEI were receiving more than 14 mm/day rainfall. The rainfall scanty zones are NWI, lower IGP, eastern SPI which received rainfall in the range of less than 2 mm/day. In term of % departure from the normal rainfall indicates that cases of extreme pIOD years may modulate the rainfall over Gujarat, Maharashtra, WG, upper Himalayan and CI part (above 35% from the normal rainfall during 35 years) on the other hand NEI, upper NWI, upper & middle IGB and eastern side of SPI region facing negative departure in ISMR (Figs. 5a–b and 6a–c). Over all pIOD effect with ENSO cause flood like situation over the WG, WPI and CI, which caused by the warmer SST along the Arabian Sea favors more moisture transport towards the subcontinent (Chaudhari et al., 2013). IOD phenomena cause a bipolarity in rainfall distribution during extreme pIOD and nIOD. During extreme nIOD, ISMR distribution was extended towards the NWI and eastern part of SPI (Fig. 5c). The ISMR departure presents a clear picture of wet and dry rainfall distribution in which CI, WPI, WG, NEI, upper Himalayan region experiences large negative departure (drought) in rainfall distribution (Figs. 5d and 6a–f).

3.5. *Simulation of Extreme pIOD and nIOD Regimes in Observation and Regional Climate Models*

RegCM4.7 model simulation with the observation rainfall illustrated in Fig. 7i–ii respectively for the extreme pIOD and nIOD years. The pIOD years 1994 and 2006 was more dominated over the central region extending towards NEI, where rainfall received by these regions are in the range of 10–20 mm/day. The WG regions experiences the surpluses amount of rainfall above 24 mm/day during major pIOD. The RCM simulation of RegCM4.7 is better in simulating pIOD year 2006 in comparison to the IMD rainfall. Therefore, the warming of Indian ocean during the strong pIOD responsible for altering the rainfall distribution over India specially over CI and NEI.

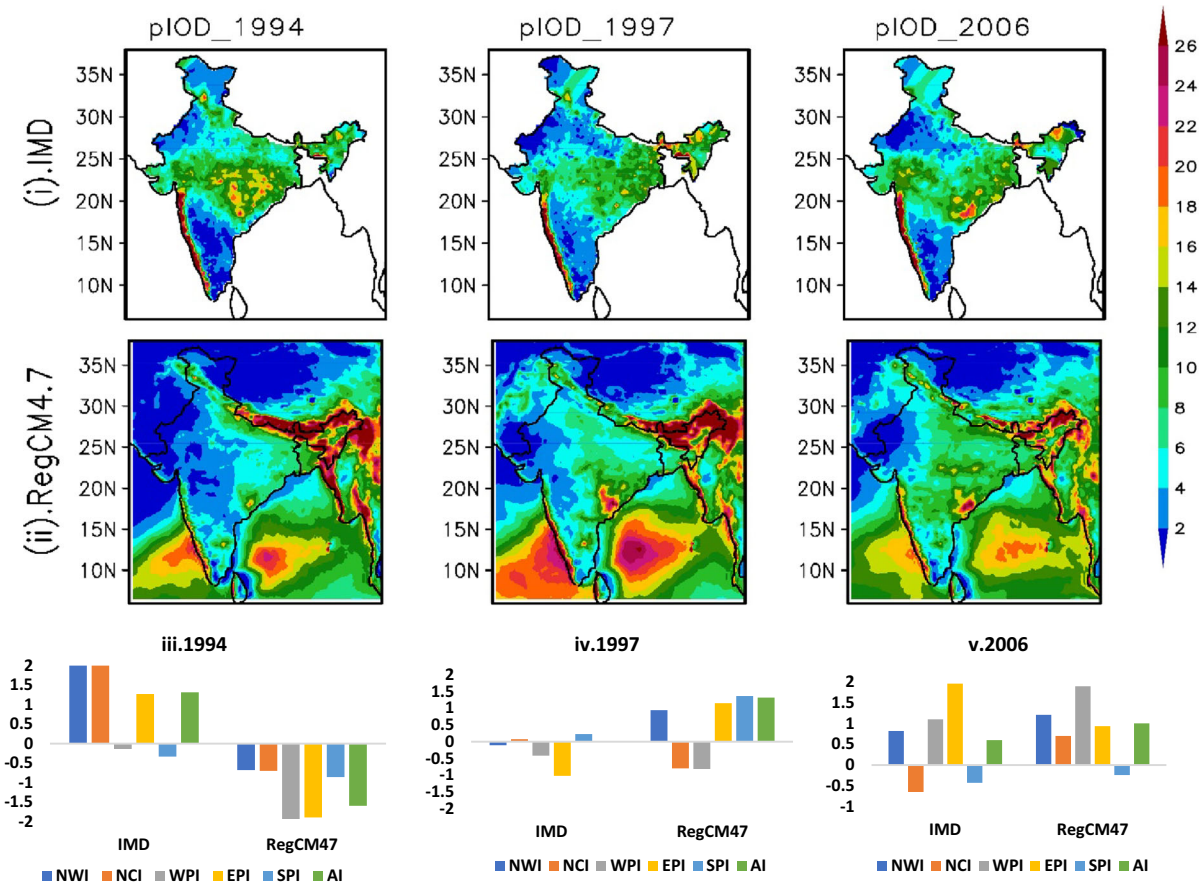

Figure 7
i–v Mean summer monsoon rainfall during extreme pIOD **i** IMD; **ii** RegCM4.7; **iii–v** standardized departure in monsoon rainfall over India and its sub regions for observation (IMD) and model simulation of RegCM4.7

The more possible description behind the significant interaction exists between the development of IOD and ENSO, a pIOD can accelerate or modify the ENSO by inducing wind anomalies associated to the walker circulation (Behera et al., 2006; Saji & Yamagata, 2003) and vice versa.

Further, in Fig. 7iii–v clearly displaying the standardised rainfall departure observed over India and its five subregions during extreme pIOD. As earlier discussed, year 1994 and 2006 experienced the above normal rainfall over all India i.e., above 2.0 standardized departure (SD) of the normal rainfall over India, in which NCI, NWI and EPI may experience flood like situation during JJAS. On the other hand, WPI and SPI region received normal ISMR, comparing these results with the RCM simulation are not up to the mark during the year 1994. In the next case scenario of 1997, strong pIOD effect nullify by strong El Nino, cause suppression of convection over the equatorial IO (Slingo & Annamalai 1999) therefore AI experiences normal rainfall except EPI region. Model simulation of RegCM4.7 are heavily affected by the ocean wide warming present in the equatorial IO, thus results are totally out of phase in compare to the observation. In the year 2006, EPI, western ghat and NEI experiencing the above 18 mm/day ISMR (Fig. 7) Also RegCM4.7 simulated precipitation pattern are matched with the IMD. The regional SD of the ISMR during 2006 depicted from Fig. 7v, also indicated that the 2006 pIOD event brings above normal rainfall over WPI and EPI which are also observed from the spatial

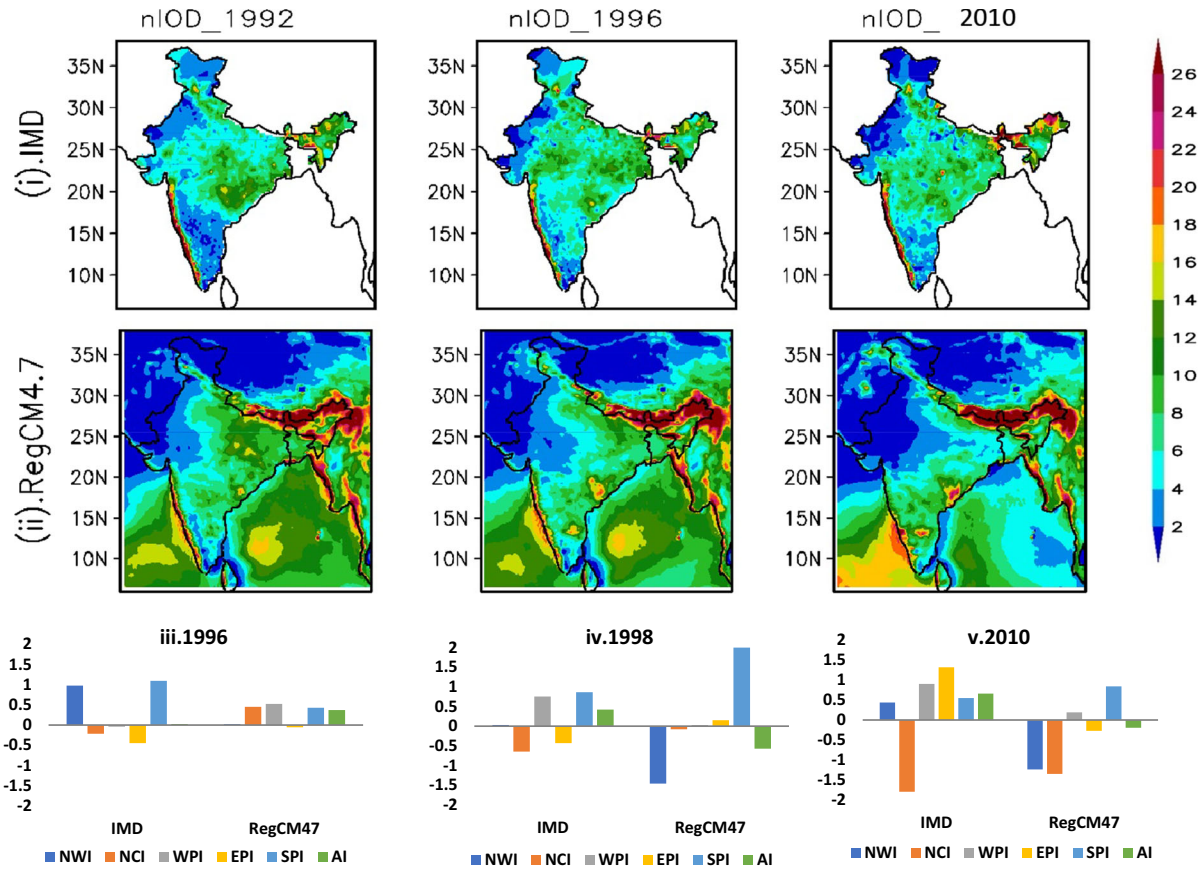

Figure 8
i–v Mean summer monsoon rainfall during extreme nIOD **i** IMD; **ii** RegCM4.7; **iii–v** standardized departure in monsoon rainfall over India and its sub regions for observation (IMD) and model simulation of RegCM4.7

rainfall plot. The model simulation over the sub regions is also similar to the observed pattern however some biasness exists but it's not out of phase.

The ISMR distribution during nIOD (1996, 1998 and 2010) has been displayed In Fig. 8i–ii for observation and model simulation of RegCM4.7. In the year 1996, India receives normal ISMR but the pattern of rainfall different from the pIOD, rainfall is dispersed homogeneously over all India. The average rainfall rate of 8–10 mm/day observed over CI, only NEI and WG showing highly intense rainfall with rate above 18 mm/day. Model simulation of RegCM4.7 are very closely resembled with the IMD rainfall. The rainfall pattern of 1996 nIOD was highly dispersed over the NWI and eastern side of SPI (which are rainfall sparse regions) in the range of 8–10 mm/day. Therefore, a common pattern of the rainfall pattern behaviours recognized that during intense nIOD event monsoon circulation might get affect and rainfall sparse zone will receive a moderate rainfall. However, rainfall departure as seen in Fig. 8iii–iv depicts that during 1996 and 1998 ISMR over the different homogenous zone was normal, only NWI and SPI receive more rainfall that its own climatology which is interesting. But the nIOD intensity and confluence with La Nina emergence its effect can cause reduction in the ISMR over the agriculture intense areas of IGP i.e., NCI specially in 2010 (Fig. 8v). The effect of 2010 strong La Nina

condition over the pacific, was nullified by the presence of moderately strong nIOD, so that normal rainfall observed all over India.

4. Conclusions

This study identified the effects of the unified response of IOD and ENSO for all India and its selected subregions, although IOD events occur irregularly and vary in strength and duration over the time period of 1981–2015. The positive and negative IOD (pIOD & nIOD) events often coincide with El Niño and La Niña events, respectively, but can occur independently. Over the monsoon core regions i.e., CI, both IOD and ENSO are the synergistic predictor for the ISMR. This study also reveals that pIOD events are stronger and becoming more frequent than nIOD events i.e., more explained by the enhanced effect of El Nino than La Nina. Also, the effect of IOD on the ISMR depends upon the developing, mature and decaying phase of ENSO. Thus, the characteristics of every El Nino and La Nina is different and intrinsic in nature, therefore, their effect on the monsoon may depend upon the regionalized details of the atmospheric response to the SST forcing especially western equatorial IO and eastern equatorial IO. Overall, the role of IO-SST, wind flow and surface pressure are more important to understand this unified/mutual response of slowly varying boundary conditions such as SST and its effect on the seasonal mean large-scale circulation of ISMR. The role of model in simulating and understanding the impact of IOD-ENSO coupling on regional rainfall pattern showed that RegCM4.7 simulated monsoon rainfall departure was highly affected during extreme pIOD (1994 and 1997). Future model simulation with the updated SST experiment might improve the simulation during extreme pIOD and nIOD.

Acknowledgements

Thanks to the India Meteorology Department (IMD) for providing the necessary datasets gridded rainfall datasets. Special thanks to International Center for Theoretical Physics (ICTP), Italy for providing RegCM4. The authors also acknowledge Institute of Eminence (IoE) Grant (Scheme No. 6031), BHU for providing funds.

Author Contributions SV, RB developed and designed the research. SV and PKS further developed the research and data analysis. SV and PKS wrote the manuscript which was subsequently modified and supervised by RB and PKS.

Funding

The authors have not disclosed any funding.

Data Availability

This study utilizes the India Meteorological Department's (IMD) daily gridded rainfall data (IMD4) with resolution of 0.25° × 0.25° over the Indian domain which is available through the 'Data SupplyPortal' (https://dsp.imdpune.gov.in/). Additionally, the RegCM4 model's initialization and boundary conditions rely on 6-hourly data from ECMWF's ERA Interim reanalysis (1.5° × 1.5° resolution) for air temperature, geopotential height, relative humidity, zonal and meridional wind (https://www.ecmwf.int/en/forecasts/datasets/reanalysisdatasets/era-interim). Furthermore, Extended Reconstructed SST, version 3b (ERSST.v3b) and sea surface salinity (SSS) ocean reanalysis dataset, known as The Ocean ReAnalysis System 5 (ORAS5) provided by the European Centre for Medium-Range Weather Forecasts (ECMWF) https://www.ecmwf.int/en/forecasts/datasets.

Declarations

Conflict of Interest The authors declare no conflict of interest.

manuscript version of this article is solely governed by the terms of such publishing agreement and applicable law.

References

Abram, N. J., Wright, N. M., Ellis, B., Dixon, B. C., Wurtzel, J. B., England, M. H., Ummenhofer, C. C., Philibosian, B., Cahyarini, S. Y., Yu, T. L., & Shen, C. C. (2020). Coupling of Indo-Pacific climate variability over the last millennium. *Nature, 579*(7799), 385–392.

Allan, R., et al. (2001). Is there an Indian Ocean dipole, and is it independent of the El Niño-Southern Oscillation? *CLIVAR Exchanges, 6*, 18–22.

Anil, N., Ramesh Kumar, M. R., Sajeev, R., & Saji, P. K. (2016). Role of distinct flavours of IOD events on Indian summer monsoon. *Natural Hazards, 82*, 1317–1326.

Annamalai, H. (2010). Moist dynamical linkage between the equatorial Indian Ocean and the South Asian monsoon trough. *Journal of the Atmospheric Sciences, 67*(3), 589–610. https://doi.org/10.1175/2009JAS2991.1

Ashok, K., Guan, Z., & Yamagata, T. (2003). A look at the relationship between the ENSO and the Indian Ocean dipole. *Journal of the Meteorological Society of Japan Series II, 81*(1), 41–56.

Ashok, K., Guan, Z., Saji, N. H., & Yamagata, T. (2004). Individual and combined influences of ENSO and the Indian Ocean dipole on the Indian summer monsoon. *Journal of Climate, 17*(16), 3141–3155. https://doi.org/10.1175/1520-0442(2004)017%3c3141:IACIOE%3e2.0.CO;2

Ashok, K., Guan, Z., & Yamagata, T. (2001). Impact of the Indian Ocean dipole on the relationship between the Indian monsoon rainfall and ENSO. *Geophysical Research Letters, 28*(23), 4499–4502.

Ashok, K., & Saji, N. H. (2007). On the impacts of ENSO and Indian Ocean dipole events on sub-regional Indian summer monsoon rainfall. *Natural Hazards, 42*(2), 273–285.

Baquero-Bernal, A., Latif, M., & Legutke, S. (2002). On dipole like variability of sea surface temperature in the tropical Indian Ocean. *Journal of Climate, 15*(11), 1358–1368.

Behera, S. K., Luo, J. J., Masson, S., Rao, S. A., Sakuma, H., & Yamagata, T. (2006). A CGCM study on the interaction between IOD and ENSO. *Journal of Climate, 19*(9), 1688–1705.

Bhatla, R., Bhattacharya, S., Verma, S., Mall, R. K., & Singh, R. S. (2023). El Nino/La Nina and IOD impact on Kharif season crops over western agro-climatic zones of India. *Theoretical and Applied Climatology*. https://doi.org/10.1007/s00704-023-04361-z

Bhatla, R., Mandal, B., Verma, S., Ghosh, S., & Mall, R. K. (2019). Performance of regional climate model in simulating monsoon onset over Indian subcontinent. *Pure and Applied Geophysics (PAGEOPH), 176*(1), 409–420. https://doi.org/10.1007/s00024-018-1910-1

Bhatla, R., Varma, P., Shruti, V., & Ghosh, S. (2020). El Nino/La Nina impact on crop production over different agro-climatic zones of indo-Gangetic plain of India. *Theoretical and Applied Climatology, 142*, 151–163. https://doi.org/10.1007/s00704-020-03284-3

Cai, W., Wang, G., Gan, B., Wu, L., Santoso, A., Lin, X., Chen, Z., Jia, F., & Yamagata, T. (2018). Stabilised frequency of extreme positive Indian Ocean dipole under 1.5 °C warming. *Nature Communications, 9*(1), 1–8.

Chattopadhyay, J., & Bhatla, R. (1996). A reexamination ENSO/anti ENSO events and simultaneous performance of the Indian summer monsoon. *Mausam, 47*(1), 59–66.

Dommenget, D., & Flöter, J. (2011). Conceptual understanding of climate change with a globally resolved energy balance model. *Climate Dynamics, 37*(11), 2143–2165.

Du, Y., & Xie, S. P. (2008). Role of atmospheric adjustments in the tropical Indian Ocean warming during the 20th century in climate models. *Geophysical Research Letters*. https://doi.org/10.1029/2008GL033631

Du, Y., Zhang, Y., Zhang, L. Y., Tozuka, T., Ng, B., & Cai, W. (2020). Thermocline warming induced extreme Indian Ocean dipole in 2019. *Geophysical Research Letters, 47*(18), e2020GL090079.

Fischer, A. S., Terray, P., Guilyardi, E., Gualdi, S., & Delecluse, P. (2005). Two independent triggers for the Indian Ocean dipole/zonal mode in a coupled GCM. *Journal of Climate, 18*(17), 3428–3449. https://doi.org/10.1175/JCLI3478.1

Giorgi, F., Coppola, E., Solmon, F., Mariotti, L., Sylla, M. B., Bi, X., Elguindi, N., Diro, G. T., Nair, V., Giuliani, G., & Turuncoglu, U. U. (2012). RegCM4: Model description and preliminary tests over multiple CORDEX domains. *Climate Research, 52*, 7–29. https://doi.org/10.3354/cr01018

Guan, Z., Ashok, K., & Yamagata, T. (2003). Summertime response of the tropical atmosphere to the Indian Ocean dipole sea surface temperature anomalies. *Journal of the Meteorological Society of Japan Series II, 81*(3), 533–561.

Guan, Z., & Yamagata, T. (2003). The unusual summer of 1994 in East Asia: IOD teleconnections. *Geophysical Research Letters*. https://doi.org/10.1029/2002GL016831

Holtslag, A. A. M., De Bruijn, E. I. F., & Pan, H. L. (1990). A high resolution air mass transformation model for short-range weather forecasting. *Monthly Weather Review, 118*(8), 1561–1575. https://doi.org/10.1175/1520-0493(1990)118%3c1561:AHRAMT%3e2.0.CO;2

Hrudya, P. H., Varikoden, H., Vishnu, R., & Kuttippurath, J. (2020). Changes in ENSO-monsoon relations from early to recent decades during onset, peak and withdrawal phases of Indian summer monsoon. *Climate Dynamics, 55*(5), 1457–1471.

Huang, B., & Kinter, J. L., III. (2002). Interannual variability in the tropical Indian Ocean. *Journal of Geophysical Research: Oceans, 107*(C11), 20–21.

Kido, S., Tozuka, T., & Han, W. (2019). Anatomy of salinity anomalies associated with the positive Indian Ocean Dipole. *Journal of Geophysical Research: Oceans, 124*(11), 8116–8139.

Kinter, J. L., Miyakoda, K., & Yang, S. (2002). Recent change in the connection from the Asian monsoon to ENSO. *Journal of Climate, 15*(10), 1203–1215.

Krishnan, R., Sundaram, S., Swapna, P., Kumar, V., Ayantika, D. C., & Mujumdar, M. (2011). The crucial role of ocean–atmosphere coupling on the Indian monsoon anomalous response during dipole events. *Climate Dynamics, 37*(1), 1–17.

Krishnaswamy, J., Vaidyanathan, S., Rajagopalan, B., Bonell, M., Sankaran, M., Bhalla, R. S., & Badiger, S. (2015). Non-stationary and non-linear influence of ENSO and Indian Ocean Dipole on the variability of Indian monsoon rainfall and extreme rain events. *Climate Dynamics, 45*(1), 175–184.

Kumar, K. K., Rajagopalan, B., & Cane, M. A. (1999). On the weakening relationship between the Indian monsoon and ENSO. *Science, 284*(5423), 2156–2159.

Lau, N. C., & Nath, M. J. (2004). Coupled GCM simulation of atmosphere–ocean variability associated with zonally asymmetric SST changes in the tropical Indian Ocean. *Journal of Climate, 17*(2), 245–265. https://doi.org/10.1175/1520-0442(2004)017%3c0245:CGSOAV%3e2.0.CO;2

Li, T., Wang, B., Chang, C. P., & Zhang, Y. (2003). A theory for the Indian ocean dipole-zonal mode. *Journal of Atmospheric Science, 60*(17), 2119–2135.

Li, Z., Lin, X., & Cai, W. (2017). Realism of modelled Indian summer monsoon correlation with the tropical Indo-Pacific affects projected monsoon changes. *Scientific Reports, 7*(1), 1–7.

Lu, B., & Ren, H. L. (2020). What caused the extreme Indian Ocean dipole event in 2019? *Geophysical Research Letters, 47*(11), e2020GL087768.

Meehl, G. A., Arblaster, J. M., & Loschnigg, J. (2003). Coupled ocean–atmosphere dynamical processes in the tropical Indian and Pacific Oceans and the TBO. *Journal of Climate, 16*(13), 2138–2158.

Pillai, P. A., & Annamalai, H. (2012). Moist dynamics of severe monsoons over South Asia: Role of the tropical SST. *Journal of the Atmospheric Sciences, 69*(1), 97–115. https://doi.org/10.1175/JAS-D-11-056.1

Reed, E. V., Cole, J. E., Lough, J. M., Thompson, D., & Cantin, N. E. (2019). Linking climate variability and growth in coral skeletal records from the Great Barrier Reef. *Coral Reefs, 38*(1), 29–43.

Saji, N. H., Goswami, B. N., Vinayachandran, P. N., & Yamagata, T. (1999). A dipole mode in the tropical Indian Ocean. *Nature, 401*(6751), 360–363.

Saji, N. H., & Yamagata, T. (2003). Possible impacts of Indian Ocean dipole mode events on global climate. *Climate Research, 25*(2), 151–169. https://doi.org/10.3354/cr025151

Sikka, D. R., & Ratna, S. (2011). On improving the ability of a high-resolution atmospheric general circulation model for dynamical seasonal prediction of the extreme seasons of the Indian summer monsoon. *Mausam, 62*(3), 339–360.

Solomon, S., Manning, M., Marquis, M. and Qin, D. (2007). *Climate change 2007-the physical science basis: Working group I contribution to the fourth assessment report of the IPCC* (Vol. 4). Cambridge university press.

Thompson, B., Gnanaseelan, C., Parekh, A., & Salvekar, P. S. (2009). A model study on oceanic processes during the Indian Ocean Dipole termination. *Meteorology and Atmospheric Physics, 105*(1), 17–27. https://doi.org/10.1007/s00703-009-0033-8

Ueda, H. (2005). Air-sea coupled process involved in stepwise seasonal evolution of the Asian summer monsoon. *Geographical Review of Japan, 78*(12), 825–841.

Vecchi, G. A., & Soden, B. J. (2007). Global warming and the weakening of the tropical circulation. *Journal of Climate, 20*(17), 4316–4340. https://doi.org/10.1175/JCLI4258.1

Verma, S., & Bhatla, R. (2021). Performance of RegCM4 for dynamically downscaling of El Nina/La Nina events during Southwest Monsoon over India and its regions. *Earth and Space Science, 8*(3), 1–18. https://doi.org/10.1029/2020EA001474

Vinayachandran, P. N., & Nanjundiah, R. S. (2009). Indian Ocean sea surface salinity variations in a coupled model. *Climate Dynamics, 33*, 245–263.

Wang, H., Kumar, A., Murtugudde, R., Narapusetty, B., & Seip, K. L. (2019). Covariations between the Indian Ocean dipole and ENSO: A modeling study. *Climate Dynamics, 53*(9), 5743–5761.

Webster, P. J., Moore, A. M., Loschnigg, J. P., & Leben, R. R. (1999). Coupled ocean–atmosphere dynamics in the Indian Ocean during 1997–98. *Nature, 401*(6751), 356–360.

Wieners, C. E., de Ruijter, W. P., Ridderinkhof, W., von der Heydt, A. S., & Dijkstra, H. A. (2016). Coherent tropical Indo-Pacific interannual climate variability. *Journal of Climate, 29*(11), 4269–4291. https://doi.org/10.1175/JCLI-D-15-0262.1

Xie, S. P., Annamalai, H., Schott, F. A., & McCreary, J. P., Jr. (2002). Structure and mechanisms of South Indian Ocean climate variability. *Journal of Climate, 15*(8), 864–878. https://doi.org/10.1175/1520-0442(2002)015%3c0864:SAMOSI%3e2.0.CO;2

Yamagata, T., Behera, S. K., Luo, J. J., Masson, S., Jury, M. R., & Rao, S. A. (2004). Coupled ocean-atmosphere variability in the tropical Indian Ocean. *Earth's Climate: the Ocean-Atmosphere Interaction Geophysical Monograph, 147*, 189–212.

Yuhong, Z., Yan, D., Shaojun, Z., Yali, Y., & Xuhua, C. (2013). Impact of Indian Ocean Dipole on the salinity budget in the equatorial Indian Ocean. *Journal of Geophysical Research: Oceans, 118*(10), 4911–4923.

Zhao, S., Jin, F. F., & Stuecker, M. F. (2019). Improved predictability of the Indian Ocean Dipole using seasonally modulated ENSO forcing forecasts. *Geophysical Research Letters, 46*(16), 9980–9990.

Zheng, X. T., Xie, S. P., Du, Y., Liu, L., Huang, G., & Liu, Q. (2013). Indian Ocean dipole response to global warming in the CMIP5 multimodel ensemble. *Journal of Climate, 26*(16), 6067–6080.

Zheng, X. T., Xie, S. P., Vecchi, G. A., Liu, Q., & Hafner, J. (2010). Indian Ocean dipole response to global warming: Analysis of ocean–atmospheric feedbacks in a coupled model. *Journal of Climate, 23*(5), 1240–1253. https://doi.org/10.1175/2009JCLI3326.1

Zuo, H., Balmaseda, M. A., Tietsche, S., Mogensen, K., & Mayer, M. (2019). The ECMWF operational ensemble reanalysis–analysis system for ocean and sea ice: A description of the system and assessment. *Ocean Science, 15*(3), 779–808.

(Received May 25, 2022, revised November 4, 2023, accepted November 21, 2023, Published online December 17, 2023)